

Measuring Hubble constant using localized and unlocalized fast radio bursts

D. H. Gao,¹ Q. Wu¹, J. P. Hu¹, S. X. Yi² X. Zhou^{3,4}, F. Y. Wang^{1,5}★

¹*School of Astronomy and Space Science, Nanjing University, Nanjing 210093, China*

²*School of Physics and Physical Engineering, Qufu Normal University, Qufu 273165, China*

³*Xinjiang Astronomical Observatory, Chinese Academy of Sciences, Urumqi 830011, China*

⁴*Xinjiang Key Laboratory of Radio Astrophysics, 150 Science1-Street, Urumqi 830011, China*

⁵*Key Laboratory of Modern Astronomy and Astrophysics (Nanjing University), Ministry of Education, Nanjing 210093, China*

Accepted XXX. Received YYY; in original form ZZZ

ABSTRACT

Hubble constant (H_0) is one of the most important parameters in the standard Λ CDM model. The measurements given by two major methods show a gap greater than 4σ , also known as Hubble tension. Fast radio bursts (FRBs) are extragalactic events with millisecond duration, which can be used as cosmological probes with high accuracy. In this paper, we constrain the Hubble constant using localized and unlocalized FRBs. The probability distributions of DM_{host} and DM_{IGM} from IllustrisTNG simulation are used. 69 localized FRBs give the constraint of $H_0 = 70.41^{+2.28}_{-2.34} \text{ km s}^{-1} \text{ Mpc}^{-1}$, which lies between early-time and late-time values, thus highlighting its individuality as a cosmological probe. We also use Monte Carlo simulation and direct sampling to calculate the pseudo redshift distribution of 527 unlocalized FRBs from CHIME observation. The median values and fixed scattered pseudo redshifts are both used to constrain Hubble constant. The corresponding constraints of H_0 from unlocalized bursts are $69.89^{+0.66}_{-0.67} \text{ km s}^{-1} \text{ Mpc}^{-1}$ and $68.81^{+0.68}_{-0.68} \text{ km s}^{-1} \text{ Mpc}^{-1}$ respectively. This result also indicates that the uncertainty of Hubble constant constraint will drop to $\sim 1\%$ if the number of localized FRBs is raised to ~ 500 . Above uncertainties only include the statistical error. The systematic errors are also discussed, and play the dominant role for the current sample.

Key words: cosmological parameters – fast radio bursts

1 INTRODUCTION

The Lambda Cold Dark Matter (Λ CDM) model, also known as the standard model of cosmology, has provided convincing explanations for numerous cosmological observation facts. Λ CDM consists of six basic cosmological parameters with more derived parameters including Hubble constant (H_0). As one of the most fundamental parameters in cosmology, H_0 describes the expansion rate of current universe (Hubble 1929), and its reciprocal $1/H_0$ gives an estimation on the age of the universe. Constraints on Hubble constant have been made with generally two distinct methods (Freedman 2021), early time probes given by Cosmic Microwave Background (CMB) and late time probes given by stars such as Cepheid-calibrated type Ia supernovae (SNe Ia). With rapidly developing telescopes, predictions given by both methods have shown increased accuracy. Planck Collaboration et al. (2020) gave prediction of $H_0 = 67.66 \pm 0.42 \text{ km s}^{-1} \text{ Mpc}^{-1}$ based on Planck cosmic microwave background power spectra with 68% confidence, while Riess et al. (2022) showed $H_0 = 73.04 \pm 1.04 \text{ km s}^{-1} \text{ Mpc}^{-1}$ with Cepheid-SNIa sample. A non-negligible gap of more than 4σ appears between both results, which is known as the "Hubble Tension" (Valentino et al. 2021; Hu & Wang 2023). It is crucial to find an independent approach to resolve the Hubble tension.

Fast radio bursts (FRBs) are extraordinarily bright radio bursts

first discovered in 2007 (Lorimer et al. 2007). With subsequent discoveries of five FRBs in several years (Keane et al. 2012; Thornton et al. 2013), FRB is universally acknowledged as a special kind of high-energy astronomical phenomena characterized by extremely high burst energy, millisecond duration and extragalactic origin (Xiao et al. 2021; Petroff et al. 2022; Zhang 2023; Wu & Wang 2024). The mechanism of FRBs remains unknown, despite different hypotheses of its origination. Still, it has been proved that almost all FRBs are originated outside Milky Way due to extraordinary burst rate and extragalactic dispersion measures (Cordes & Chatterjee 2019). Some FRBs are observed multiple times while others have not shown repetitiveness for now. FRBs occur at an extreme rate, and with more telescopes searching for FRBs, observed FRBs are significantly increasing while a small yet growing proportion of FRBs are well localized with host galaxy and a definite redshift z_{FRB} .

To employ FRBs as cosmological probes, dispersion measure (DM) is a characteristic property defined as the integral of electron number density along the path of propagation, i.e. $DM = \int_0^d n_e(l) dl$. By precisely determining DM, especially component contributed by intergalactic medium (DM_{IGM}), FRBs could be used as high-accuracy probes in multiple cases (Bhandari & Flynn 2021; Wu & Wang 2024), such as measuring the Hubble constant (Wu et al. 2022; Hagstotz et al. 2022; James et al. 2022; Zhao et al. 2022; Wei & Melia 2023; Gao et al. 2024) and Hubble parameter (Wu et al. 2020), dark energy (Zhou et al. 2014; Walters et al. 2018; Kumar & Linder 2019; Qiu et al. 2022), and bounding the photon rest mass

★ E-mail: fayinwang@nju.edu.cn

(Wang et al. 2021; Lin et al. 2023; Wang et al. 2024), measuring reionization history (Zhang et al. 2021; Bhattacharya et al. 2021), probing compact dark matter (Muñoz et al. 2016; Wang & Wang 2018), and finding missing baryons (Walters et al. 2018; Li et al. 2020; Macquart et al. 2020a; Yang et al. 2022; Lin & Zou 2023; Wang & Wei 2023; Connor et al. 2024). Early researches assume dispersion measures contributed by intergalactic medium (DM_{IGM}) and host galaxy (DM_{host}) to be certain values, though it is practically not possible to distinguish the partition between DM_{IGM} and DM_{host} . Macquart et al. (2020b) and Zhang et al. (2021) provided a possible solution of considering the probability density distributions for DM_{IGM} and DM_{host} to solve "degeneracy problem". Several works have been done to constrain H_0 with FRBs, such as Wu et al. (2022) using 18 localized bursts to get a constraint of 8% uncertainty, Hagstotz et al. (2022) measuring H_0 from localized FRBs assuming a constant value of DM_{host} , James et al. (2022) using data from Australian Square Kilometer Array Pathfinder and Parkes to get a result of 10.9% uncertainty, Zhao et al. (2022) using 12 unlocalized FRBs to constrain H_0 by identifying host galaxies with probability distributions, and Kalita et al. (2024) using 64 localized FRBs to constrain H_0 with different models of IGM and host galaxy.

In this paper, we constrain Hubble constant with 69 localized FRBs and 527 unlocalized FRBs, and predict the confidence interval of Hubble constant assuming all 527 FRBs are well localized. In Section 2 we introduce the theoretical model used for DMs of FRBs. In Section 3 we show our Markov Chain Monte Carlo model and give the constraint given by localized FRBs. In Section 4 we propose the pseudo redshift of unlocalized FRBs and give corresponding result. In Section 5 we discuss the statistical and systematic error of our result.

2 DISTRIBUTION OF DISPERSION MEASURES

Generally, the dispersion measures of FRBs could be broken down into following components:

$$DM_{\text{obs}} = DM_{\text{ISM}} + DM_{\text{halo}} + DM_{\text{IGM}} + \frac{DM_{\text{host}}}{1+z}, \quad (1)$$

where DM_{obs} is total observed DM, while DM_{ISM} , DM_{halo} , DM_{IGM} and DM_{host} refers to DM contributed by interstellar medium (ISM) within Milky Way, galactic halo, intergalactic medium and host galaxy of FRB respectively.

2.1 Galactic dispersion measures

The former two components, DM_{ISM} and DM_{halo} , are contributed by medium within Milky Way and also referred to as a whole, i.e. $DM_{\text{MW}} = DM_{\text{ISM}} + DM_{\text{halo}}$. DM_{ISM} could be well described by galactic electron distribution models such as YMW16 by Yao et al. (2017) and NE2001 by Cordes & Lazio (2002). According to Ocker et al. (2021), YMW16 might overestimate DM_{ISM} for FRBs in the direction of anticenter and possibly other low-latitude bursts. The difference between NE2001 and YMW16 may have little influence on constraint of H_0 (Wu et al. 2022), still we apply NE2001 to estimate DM_{ISM} as previous researchers do. Prochaska & Zheng (2019) gave the constraint of $DM_{\text{halo}} = 50\sim 80 \text{ pc cm}^{-3}$ based on multiple observation data. It is reasonable to assume that DM_{halo} follows a Gaussian distribution with $\langle DM_{\text{halo}} \rangle = 65 \text{ pc cm}^{-3}$ and $\sigma = 15 \text{ pc cm}^{-3}$. To reduce calculation and avoid another level of integration, we simplify DM_{halo} to be its mean value, i.e. $DM_{\text{halo}} = 65 \text{ pc cm}^{-3}$, which should have minor influence on our estimation since the halo component appears as linear form in $DM_{\text{exc}} = DM_{\text{obs}} - DM_{\text{ISM}} - DM_{\text{halo}}$.

2.2 Extragalactic dispersion measures

As discussed in Section 2.1, contributions from within our Galaxy can be well estimated with galactic electron models, we subtract DM_{MW} from total DM to obtain the extragalactic component:

$$DM_{\text{exc}} = DM_{\text{obs}} - DM_{\text{MW}} = DM_{\text{IGM}} + \frac{DM_{\text{host}}}{1+z}. \quad (2)$$

DM_{host} is the dispersion measure contributed by host galaxy of FRB source, and its probability distribution can be fitted by a lognormal distribution according to Macquart et al. (2020b). The intergalactic component DM_{IGM} could be described with a Gaussian-like distribution around its mean value. In a standard Λ CDM universe model, the mean value of DM_{IGM} is given by Deng & Zhang (2014) as:

$$\langle DM_{\text{IGM}} \rangle = \frac{3cH_0\Omega_b f_{\text{IGM}}}{8\pi G m_p} \times f_e(z), \quad (3)$$

where m_p is proton mass, f_{IGM} is the fraction of baryon in IGM. Previous researches prefer a value of $f_{\text{IGM}} \approx 0.84$ according to Shull et al. (2012), yet Connor et al. (2024) gives a more accurate constraint of $f_{\text{IGM}} \approx 0.93$ with data from the Deep Synoptic Array (DSA-110) using both FRB and non-FRB methods (notably what we called f_{IGM} corresponds to f_d instead of f_{IGM} in their research). We adopt the value of $f_{\text{IGM}} = 0.93$ in our simulation. The integral $f_e(z)$ is defined as:

$$f_e(z) = \int_0^z \frac{\left[\frac{3}{4}y_1\chi_{e,\text{H}}(z) + \frac{1}{8}y_2\chi_{e,\text{He}}(z) \right] (1+z) dz}{\left[\Omega_m(1+z)^3 + \Omega_\Lambda \right]^{1/2}}. \quad (4)$$

The cosmological parameters Ω_m and Ω_Λ are given by Planck 2018 results (Planck Collaboration et al. 2020), and we have $\Omega_\Lambda = 1 - \Omega_m$ assuming a flat universe. Ω_b is decided as an assumption in Planck results based on big bang nucleosynthesis (BBN) constraints and primordial deuterium abundance measurements by Cooke et al. (2018), which is always given in the form of $\Omega_b h^2$ where $h = H_0/100 \text{ km s}^{-1} \text{ Mpc}^{-1}$, thus we modify the equation to keep Ω_b in the form of $\Omega_b H_0^2$. y_1 and y_2 in Equation (4) are hydrogen and helium fractions normalized to 0.75 and 0.25 respectively, which can be neglected as $y_1 \approx y_2 \approx 1$. $\chi_{e,\text{H}}(z)$ and $\chi_{e,\text{He}}(z)$ are ionization fraction of hydrogen and helium, which could also be considered to be $\chi_{e,\text{H}}(z) = \chi_{e,\text{He}}(z) = 1$ at $z < 3$. Equations (3) and (4) can now be further rewritten as:

$$\langle DM_{\text{IGM}} \rangle = \frac{21c\Omega_b H_0^2}{64\pi H_0 G m_p} \times \int_0^z \frac{f_{\text{IGM}}(1+z) dz}{\left[\Omega_m(1+z)^3 + 1 - \Omega_m \right]^{1/2}}. \quad (5)$$

3 MONTE CARLO SIMULATION AND CONSTRAINT WITH LOCALIZED FRBS

3.1 Monte Carlo simulation

To run a Markov Chain Monte Carlo (MCMC) simulation, the probability distribution of extragalactic DM components must be calculated. As described in Section 2.2, DM_{host} follows a lognormal distribution while DM_{IGM} can be fitted with a Gaussian-like distribution, which often writes as (McQuinn 2013; Macquart et al. 2020b):

$$p_{\text{host}}(DM_{\text{host}}) = \frac{1}{\sqrt{2\pi} DM_{\text{host}} \sigma_{\text{host}}} \exp \left[-\frac{(\ln DM_{\text{host}} - \mu)^2}{2\sigma_{\text{host}}^2} \right] \quad (6)$$

$$p_{\text{IGM}}(\Delta) = A\Delta^{-\beta} \exp \left[-\frac{(\Delta^{-\alpha} - C_0)^2}{2\alpha^2\sigma_{\text{IGM}}^2} \right], \quad \Delta = \frac{DM_{\text{IGM}}}{\langle DM_{\text{IGM}} \rangle}, \quad (7)$$

where α and β are parameters indicating inner density profile of halo gas, and [Macquart et al. \(2020b\)](#) proposed the best-fitting result of $\alpha = \beta = 3$. A and C_0 are normalization parameters given by $\int p_{\text{IGM}} = 1$ and $\langle \Delta \rangle = 1$, while σ_{host} , μ and σ_{IGM} are distribution parameters respectively. e^μ is generally chosen as distribution parameter instead of μ , since e^μ indicates mean value of DM_{host} .

One possible way of further simulation to determine H_0 is to fit all undetermined parameters at the same time, and the probability function goes like:

$$p \sim p_{\text{host}}(\text{DM} | e^\mu, \sigma_{\text{host}}, H_0) p_{\text{IGM}}(\text{DM} | \sigma_{\text{IGM}}, H_0). \quad (8)$$

Still, since the number of localized FRBs is limited ($n_{\text{local}} < 50$), the confidence may be weakened to fit a four-dimensional parameter space ($e^\mu, \sigma_{\text{host}}, \sigma_{\text{IGM}}, H_0$) with current data. Another concern is that distribution parameters are not fixed constant for different FRBs, and some have shown redshift-dependent. [Zhang et al. \(2020\)](#) and [Zhang et al. \(2021\)](#) proposed the best-fitted distribution parameters of DM_{host} and DM_{IGM} derived from IllustrisTNG Simulation ([Pillepich et al. 2017](#)), which takes redshift-dependent evolution into consideration as well. [Zhang et al. \(2021\)](#) also provided the evolution of A and C_0 , and it is shown that the best-fitted value slightly deviates from normalization. To apply results above, all localized FRBs are divided roughly into three categories based on host galaxy: (a) non-repeating (one-off) bursts; (b) FRB121102-like repeating bursts: host galaxy stellar mass $\approx 4 \sim 7 \times 10^7 M_\odot$, star formation rate (SFR) ≈ 0.4 ; (c) FRB180916-like repeating bursts: host galaxy stellar mass $\approx 10^{10} M_\odot$, SFR ≈ 0.016 . Note that this classification only indicates qualitative properties of the host galaxy and is not absolute. [Zhang et al. \(2020\)](#) and [Zhang et al. \(2021\)](#) provided best-fitted values of distribution parameters at several typical redshifts, and we perform a monotone cubic spline interpolation for each parameter to obtain values at any given redshift.

By obtaining values for ($e^\mu, \sigma_{\text{host}}, \sigma_{\text{IGM}}, A, C_0$) from IllustrisTNG, the only free parameter left is H_0 , which is what we are interested in. Taking all parameters into Equation (6) and (7), we have the likelihood function for any single FRB:

$$\mathcal{L}_{\text{FRB}} = \int_0^{(1+z)(\text{DM}_{\text{obs}} - \text{DM}_{\text{MW}})} p_{\text{host}}(\text{DM}_{\text{host}} | H_0) \times p_{\text{IGM}}(\text{DM}_{\text{obs}} - \text{DM}_{\text{MW}} - \frac{\text{DM}_{\text{host}}}{(1+z)} | H_0) d \text{DM}_{\text{host}}. \quad (9)$$

Though not wrote explicitly, the distribution parameters in Equation (9) are distinct for each burst. For the i^{th} FRB, the complete likelihood function is:

$$\mathcal{L}_i = \mathcal{L}_i(\text{DM}_{\text{obs}}^{(i)} | H_0, \text{DM}_{\text{MW}}^{(i)}, z_i, e_i^\mu, \sigma_{\text{host}}^{(i)}, \sigma_{\text{IGM}}^{(i)}, A_i, C_{0,i}), \quad (10)$$

and the total log-likelihood function of all FRBs is:

$$\ln \mathcal{L}(H_0) = \sum_{i=1}^n \ln \mathcal{L}_i(\text{DM}_{\text{obs}}^{(i)} | H_0). \quad (11)$$

According to Bayesian theory, we still need a prior of H_0 to perform parameter estimation, and we use a uniform distribution $H_0 \in \mathcal{U}(0, 100) \text{ km s}^{-1} \text{Mpc}^{-1}$ as its prior.

3.2 Simulation of localized FRBs

3.2.1 Data preprocessing

As discussed in Section 1, the host galaxies of a few FRBs have been determined by different methods. We collected data of all localized FRBs as of now, including FRBs newly localized by DSA-110 ([Connor et al. 2024](#)), and list in Table 1, with equatorial coordinates and

dispersion measures of bursts as well as the redshift of host galaxy. All FRBs are classified into three types based on their host galaxies. It should be noted that DM_{host} can be further divided into two components, which are contributed by host galaxy and FRB source respectively. FRBs such as FRB20190520B and FRB20220831A are considered to have extreme $\text{DM}_{\text{source}}$, which are not suitable to use in our constraint and may cause significant inaccuracy. FRBs like FRB20181030, FRB20200120E, FRB20220319D, FRB20210405I and FRB20201123A are excluded due to such large DM_{MW} that $\text{DM}_{\text{exc}} < \text{DM}_{\text{MW}}$ or even $\text{DM}_{\text{exc}} < 0$. FRB20221027A is excluded for its ambiguity in host galaxy localization.

To run Monte Carlo simulation, we use open-source python package `emcee`, which is a python implementation of [Goodman & Weare \(2010\)](#). For cosmological parameters, we use the value given by [Planck Collaboration et al. \(2020\)](#) Table 2 (TT, TE, EE + lowE + lensing + BAO), i.e. $\Omega_b h^2 = 0.02242 \pm 0.00014$, $\Omega_\Lambda = 0.6889 \pm 0.0056$, $\Omega_m = 0.3111 \pm 0.0056$. For other parameters, we adopt $f_{\text{IGM}} = 0.93$, $\text{DM}_{\text{halo}} = 65 \text{ pc cm}^{-3}$. The statistical error of these predetermined parameters will be discussed in Section 5. At the very beginning of simulation, the observation data are preprocessed, which includes:

(a) Calculating galactic component of dispersion measures and subtracting it from total DM to obtain DM_{exc} ;

(b) Performing monotone cubic spline interpolations on data from [Zhang et al. \(2020, 2021\)](#) and calculating distribution parameters involved in Equation (10) for each FRB;

(c) Setting initial positions for MCMC walkers. A universal choice for initialization is to uniformly scatter walkers in a small sphere around the optimal value given by maximum likelihood estimation (MLE). We tested intervals with length of $10^{-3} \text{ km s}^{-1} \text{Mpc}^{-1}$ centering at different values within $[65, 72] \text{ km s}^{-1} \text{Mpc}^{-1}$, and found that initialization has little influence on simulation result. Even simulations initialized with values majorly deviated from $\sim 70 \text{ km s}^{-1} \text{Mpc}^{-1}$ (for example, initialized within $80 \pm 10^{-3} \text{ km s}^{-1} \text{Mpc}^{-1}$) could converge within < 30 MCMC steps. We use $\mathcal{U}(70 - 10^{-3}, 70 + 10^{-3}) \text{ km s}^{-1} \text{Mpc}^{-1}$ as our final initialization.

3.2.2 Monte Carlo cycle and postprocessing

After preprocessing FRB data, we can run Monte Carlo simulation. We set up a Monte Carlo system with 512 walkers, and within each Monte Carlo cycle, the program will go through following steps:

(a) Calculate mean value of DM_{IGM} with current H_0 based on Equation (5) for each FRB;

(b) For any given DM_{host} , calculate $p_{\text{host}}(\text{DM}_{\text{host}})$ and $p_{\text{IGM}}(\Delta)$ based on Equation (6) and (7), and integrate DM_{host} to get likelihood function \mathcal{L}_{FRB} according to Equation (9) for each FRB;

(c) Sum log-likelihood functions of all FRBs, and update H_0 based on total likelihood.

The autocorrelation time τ_f is a typical value integrated from autocorrelation function (ACF) to indicate whether the system converges. Documentation of `emcee` and [Goodman & Weare \(2010\)](#) suggests that $N > 50\tau$ would be long enough where N is the length of MCMC chain. We run a chain of 2000 steps and the autocorrelation time is $\tau = 24.33$. We discard the first $\lceil \tau + 50 \rceil$ steps that may not converge well and flatten following steps to get a total of $1925 \times 512 = 985600$ samples.

Table 1. Data of localized FRBs. FRB type shows whether an event is an one-off burst (type = 3) or a repeated burst (type = 1 or 2). Furthermore, type = 1 indicates a 20121102-like burst while type = 2 indicates a 20180916-like burst. FRB20190520B and FRB20220831A may have extreme DM_{source} and are not suitable for constraining. FRB20181030, FRB20200120E, FRB20220319D, FRB20210405I and FRB20201123A are excluded due to too large DM_{MW} . FRB20221027A is excluded for its ambiguity in host galaxy localization.

FRB Type	TNS Name	RA	DEC	DM (pc cm ⁻³)	Redshift	Reference
1	FRB20121102	5:31:58	+33:08:04	557	0.1927	Tendulkar et al. (2017) Chatterjee et al. (2017)
1	FRB20180301	6:12:54.44	+4:40:15.8	536	0.3304	Bhandari et al. (2022)
2	FRB20180916	1:58:00.75	+65:43:00.32	348.76	0.0337	Marcote et al. (2020)
3	FRB20180924	21:44:25.3	-40:54:00.1	361.42	0.3214	Bannister et al. (2019)
1	FRB20181030 (Unused)	10:34:20.1	+73:45:05	103.5	0.0039	Bhardwaj et al. (2021)
2	FRB20180814	4:22:56.01	+73:39:40.7	189.4	0.068	Michilli et al. (2023)
3	FRB20181112	21:49:23.63	-52:58:15.39	589.27	0.4755	Prochaska et al. (2019)
3	FRB20190102	21:29:39.76	-79:28:32.5	364.5	0.2913	Bhandari et al. (2020)
1	FRB20190303A	13:51:58	+48:7:20	222.4	0.064	Michilli et al. (2023)
3	FRB20190523	13:48:15.6	+72:28:11	760.8	0.66	Ravi et al. (2019)
3	FRB20190608	22:16:04.74	-7:53:53.6	339.5	0.11778	Chittidi et al. (2021)
3	FRB20190611	21:22:58.91	-79:23:51.3	321.4	0.378	Heintz et al. (2020)
3	FRB20190614	4:20:18.13	+73:42:22.9	959.2	0.6	Law et al. (2020)
1	FRB20190711	57:40.7	-80:21:28.8	593.1	0.522	Heintz et al. (2020)
3	FRB20190714	12:15:55.12	-13:01:15.7	504.13	0.2365	Heintz et al. (2020)
3	FRB20191001	21:33:24.373	-54:44:51.43	507.9	0.234	Heintz et al. (2020)
3	FRB20191228	22:57:43.3	-29:35:38.7	297.5	0.2432	Bhandari et al. (2022)
3	FRB20200430	15:18:49.54	+12:22:36.8	380.25	0.16	Heintz et al. (2020)
3	FRB20200906	3:3:59.08	-14:04:59.5	577.8	0.3688	Bhandari et al. (2022)
2	FRB20201124	5:08:03.5	+26:03:38.4	413.52	0.098	Ravi et al. (2022)
1	FRB20190520B (Unused)	16:02:04.266	-11:17:17.33	1210.3	0.241	Niu et al. (2022)
3	FRB20200120E (Unused)	9:57:54.7	+68:49:0.9	87.8	0.0008	Kirsten et al. (2022)
3	FRB20210117A	22:39:55.015	-16:09:05.45	728.95	0.214	Bhandari et al. (2023)
3	FRB20220610A	23:24:17.569	-33:30:49.37	1457.624	1.016	Ryder et al. (2023)
2	FRB20220912A	23:09:04.9	+48:42:25.4	219.46	0.0771	Ravi et al. (2023b)
3	FRB20220319D (Unused)	08:42.7	+71:02:06.9	110.95	0.0111	Ravi et al. (2023a)
3	FRB20210410D	21:44:20.7	-79:19:05.5	578.78	0.1415	Caleb et al. (2023)
3	FRB20210405I (Unused)	17:01:21.5	-49:32:42.5	565.17	0.066	Driessen et al. (2023)
3	FRB20220207C	20:40:47.886	+72:52:56.378	262.38	0.04304	Law et al. (2024)
3	FRB20220307B	23:23:29.88	+72:11:32.6	499.27	0.248123	Law et al. (2024)
3	FRB20220310F	8:58:52.9	+73:29:27.0	462.24	0.477958	Law et al. (2024)
3	FRB20220418A	14:36:25.34	+70:05:45.4	623.25	0.622	Law et al. (2024)
3	FRB20220506D	21:12:10.76	+72:49:38.2	396.97	0.30039	Law et al. (2024)
3	FRB20220509G	18:50:40.8	+70:14:37.8	269.53	0.0894	Law et al. (2024)
3	FRB20220825A	20:47:55.55	+72:35:05.9	651.24	0.241397	Law et al. (2024)
3	FRB20220914A	18:48:13.63	+73:20:12.9	631.28	0.1139	Law et al. (2024)
3	FRB20220920A	16:01:01.70	+70:55:07.7	314.99	0.158239	Law et al. (2024)
3	FRB20221012A	18:43:11.69	+70:31:27.2	441.08	0.284669	Law et al. (2024)
3	FRB20210603A	0:41:05.774	+21:13:34.573	500.147	0.177	Cassanelli et al. (2023)
3	FRB20210320C	-	-	384.8	0.2797	Shannon(in prep.)
3	FRB20211127I	-	-	234.83	0.0469	Deller(in prep.)

Table 1. (continued)

FRB Type	TNS Name	RA	DEC	DM (pc cm ⁻³)	Redshift	Reference
3	FRB20211212A	-	-	206	0.0715	Deller(in prep.)
1	FRB20240114A	21:27:39.835	+4:19:45.634	527.7	0.13	Chen(in prep.)
3	FRB20171020A	22:15:24.75	-19:35:07.00	114.1	0.0087	Mahony et al. (2018)
3	FRB20201123A (Unused)	17:34:40.8	-50:40:12	433.55	0.0507	Rajwade et al. (2022)
3	FRB20210807D	19:56:53.14	-00:45:44.50	251.3	0.1293	Deller(in prep.)
3	FRB20211203C	13:38:15.00	-31:22:48.20	635	0.3439	Gordon et al. (2023)
3	FRB20220105A	13:55:12.94	+22:27:59.40	580	0.2785	Gordon et al. (2023)
1	FRB20220529A	01:16:25.01	+20:37:57.03	246	0.183900	Li(in prep.)
3	FRB20220204A	18:16:54.30	+69:43:21.01	612.2	0.4	Connor et al. (2024)
3	FRB20220208A	21:30:18.03	+70:02:27.75	437	0.351	Connor et al. (2024)
3	FRB20220330D	10:55:00.30	+70:21:02.70	468.1	0.3714	Connor et al. (2024)
3	FRB20220726A	04:55:46.96	+69:55:44.80	686.55	0.361	Connor et al. (2024)
3	FRB20220831A (unused)	22:34:46.93	+70:13:56.50	1146.25	0.262	Sharma et al. (2024)
3	FRB20221027A (unused)	08:43:29.23	+72:06:03.50	452.5	0.229	Connor et al. (2024)
3	FRB20221029A	09:27:51.22	+72:27:08.34	1391.05	0.975	Connor et al. (2024)
3	FRB20221101B	22:48:51.89	+70:40:52.20	490.7	0.2395	Connor et al. (2024)
3	FRB20221113A	04:45:38.64	+70:18:26.60	411.4	0.2505	Connor et al. (2024)
3	FRB20221116A	01:24:50.45	+72:39:14.10	640.6	0.2764	Connor et al. (2024)
3	FRB20221219A	17:10:31.15	+71:37:36.63	706.7	0.554	Connor et al. (2024)
3	FRB20230124	15:27:39.90	+70:58:05.20	590.6	0.094	Connor et al. (2024)
3	FRB20230216A	10:25:53.32	+03:26:12.57	828	0.531	Connor et al. (2024)
3	FRB20230307A	11:51:07.52	+71:41:44.30	608.9	0.271	Connor et al. (2024)
3	FRB20230501A	22:40:06.52	+70:55:19.82	532.5	0.301	Connor et al. (2024)
3	FRB20230521B	23:24:08.64	+71:08:16.91	1342.9	1.354	Sharma et al. (2024)
3	FRB20230626A	15:42:31.10	+71:08:00.77	451.2	0.327	Connor et al. (2024)
3	FRB20230628A	11:07:08.81	+72:16:54.64	345.15	0.1265	Connor et al. (2024)
3	FRB20230712A	11:09:26.05	+72:33:28.02	586.96	0.4525	Connor et al. (2024)
3	FRB20230814A	22:23:53.94	+73:01:33.26	696.4	0.5535	Sharma et al. (2024)
3	FRB20231120A	09:35:56.15	+73:17:04.80	438.9	0.07	Connor et al. (2024)
3	FRB20231123B	16:10:09.16	+70:47:06.20	396.7	0.2625	Connor et al. (2024)
3	FRB20231220A	08:15:38.09	+73:39:35.70	491.2	0.3355	Sharma et al. (2024)
3	FRB20240119A	14:57:52.12	+71:36:42.33	483.1	0.37	Sharma et al. (2024)
3	FRB20240123A	04:33:03.00	+71:56:43.02	1462	0.968	Sharma et al. (2024)
3	FRB20240213A	11:04:40.39	+74:04:31.40	357.4	0.1185	Sharma et al. (2024)
3	FRB20240215A	17:53:45.90	+70:13:56.50	549.5	0.21	Sharma et al. (2024)
3	FRB20240229A	11:19:56.05	+70:40:34.40	491.15	0.287	Sharma et al. (2024)

3.2.3 Results of localized FRBs

The histogram of all samples is plotted with bin-width chosen according to Freedman Diaconis rule implemented by `numpy`, and the probability density function (PDF) is given by kernel density estimation (KDE). We also plot cumulative histogram to get the cumulative distribution function (CDF), and the 1σ confidence interval is $H_0 = 70.41^{+2.28}_{-2.34}$ km s⁻¹Mpc⁻¹ as shown in Fig. 1. Our constraint from localized FRBs lies between early-time result given by Planck

Collaboration et al. (2020) and late-time result given by Riess et al. (2022), which supports that FRBs can be used as individual cosmological probes to constrain H_0 .

4 CONSTRAINT WITH UNLOCALIZED FRBS

Though the number of localized FRBs is increasing rapidly, an absolute majority still remain unlocalized, therefore it is crucial to utilize

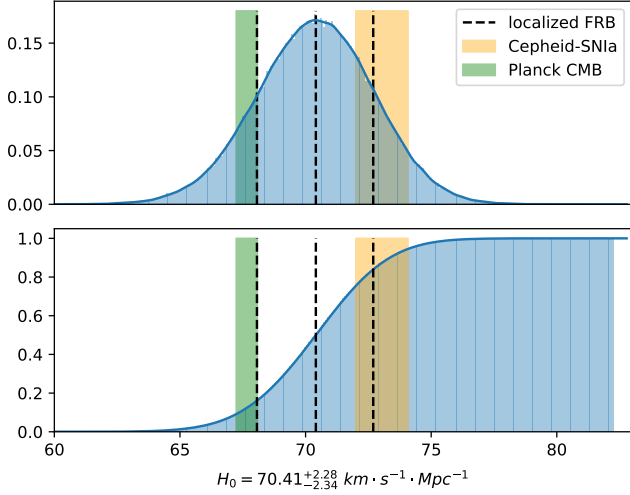


Figure 1. PDF and CDF of Hubble constant given by 69 localized FRBs in Table 1. Vertical line shows our result $H_0 = 70.41^{+2.28}_{-2.34} \text{ km} \cdot \text{s}^{-1} \cdot \text{Mpc}^{-1}$ with 1σ uncertainty. Orange and green regions are 1σ confidence intervals by SNIa and CMB respectively.

unlocalized FRBs. A common solution is to inverse "pseudo redshifts" with observed DM (Tang et al. 2023). Compared with another method of simply generating FRB data with simulation, FRBs with pseudo redshift are not dependent on any pre-assumption of DM distribution, and use real DM data as its foundation. We collect data of unlocalized FRBs from CHIME database. We used all bursts in CHIME catalog 1 (CHIME/FRB Collaboration et al. 2021) and part of available repetitive bursts with definite coordinates in CHIME catalog 2023 (Chime/Frb Collaboration et al. 2023) to run MCMC simulation. Note that when processing repetitive FRBs, we consider all bursts from the same source as one single event, and calculate their mean DM as DM_{obs} . With pseudo redshifts, we could utilize all unlocalized FRBs as localized ones to constrain Hubble constant.

4.1 Pseudo redshift

4.1.1 Circular argument

Before estimating pseudo redshifts, a pre-determined value for H_0 is required, which may lead to a "circular argument" by assuming H_0 to be a certain value while calculating H_0 . However it can be considered as an iterative analysis similar to Newton-Raphson method, where we assume an initial value $H_0^{(0)}$ to calculate pseudo redshift $z^{(0)}$, and apply $z^{(0)}$ to estimate $H_0^{(1)}$. To be precise, this step should repeat as

$$H_0^{(0)} \rightarrow z^{(0)} \rightarrow H_0^{(1)} \rightarrow z^{(1)} \rightarrow \dots \rightarrow H_0^{(n)} \rightarrow z^{(n)} \quad (12)$$

until $|H_0^{(n)} - H_0^{(n+1)}| < \varepsilon$. Yet we find that the difference of initial value for H_0 has little influence on pseudo redshift and therefore even less influence on final estimation of H_0 , and our initial value is actually close enough with final result ($\Delta H_0/H_0 \sim 1.4\%$), thus we skip the latter parts in Equation (12).

Another way to avoid circular argument is to consider H_0 as an unfitted parameter same as pseudo redshift instead of pre-assuming its value. To guarantee that the fit H_0 is the same for all FRBs, it is required to calculate pseudo redshift for all FRBs at the same time, i.e. to fit $(H_0, z_1, z_2, \dots, z_n)$ simultaneously. For $n = 527$, an enormous computational resource is required to fit a 528-dimensional parameter

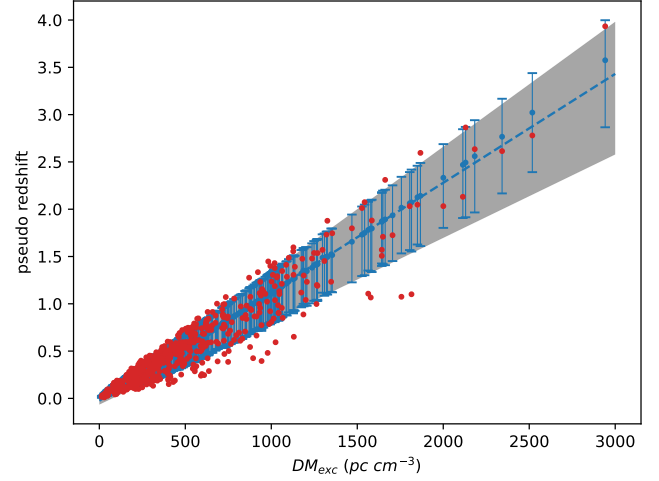


Figure 2. Estimated pseudo redshifts of unlocalized FRBs in CHIME catalog. Blue dots with errorbars are 16%, 50% and 84% percentiles of redshift estimated by MCMC simulation. Blue dashed line and grey region are fitted from percentiles. Red dots are estimated pseudo redshift, which is randomly decided based on probability distribution function given by MCMC simulation for each FRB. Extreme MCMC samples are neglected, i.e., samples below 3% or above 97% among all 1152 thinned samples are discarded when calculating the possibility distribution function.

space. In comparison, we could run 527 individual simulations using Equation (12), and fit pseudo redshift for each FRB at a time, which can significantly reduce computation.

4.1.2 Calculating pseudo redshifts

To estimate pseudo redshifts, there are two different methods: maximum likelihood estimation and Monte Carlo simulation. Both methods require a likelihood function slightly different from Equation 9. H_0 is now a known parameter while z_i is the unfitted variable. The equation is rewrite as:

$$\mathcal{L}(z_i) = \int_0^{(1+z_i)(\text{DM}_i - \text{DM}_{\text{MW}})} p_{\text{host}}(\text{DM}_{\text{host}} | z_i) \times p_{\text{IGM}}(\text{DM}_i - \text{DM}_{\text{MW}} - \frac{\text{DM}_{\text{host}}}{(1+z_i)} | z_i) d \text{DM}_{\text{host}}. \quad (13)$$

MLE can give the mean value of pseudo redshift for each FRB, yet the chain may fail to converge for FRBs with extremely low dispersion measure ($\text{DM} \sim 100 \text{ pc cm}^{-3}$), and MLE gives no information about its distribution. Monte Carlo simulation provides probability density distribution and works for FRBs with low DM.

With similar MCMC simulation as described in Section 3.2.2, 57600 samples ($n_{\text{walkers}}=64$, discard=100, steps=1000) are generated for each single FRB. We calculate the 16, 50, 84 percentile of pseudo redshift for each FRB and plot them in the form of errorbar on a scatterplot with dispersion measure as horizontal axis. For any given percentile (z_{16}, z_{50} or z_{84} for example), $z \sim \text{DM}_{\text{exc}}$ shows a good linear relation, which agrees with pseudo redshift result in previous researches. We plot result of linear regression and show the 68% confidence region in Fig. 2.

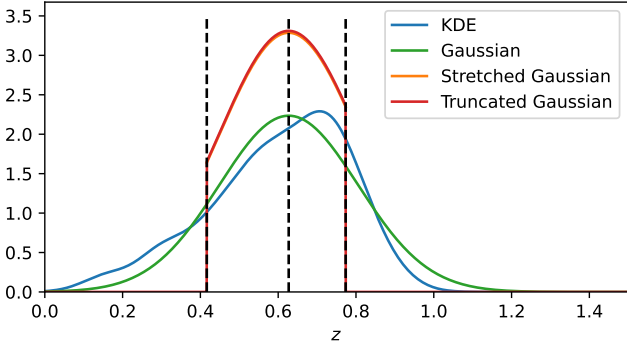


Figure 3. Comparison of different distribution functions in fitting pseudo redshift of FRB20180725A ($DM_{\text{exc}} = 644.2 \text{ pc cm}^{-3}$). Vertical lines are 68% confidence interval (1σ) of pseudo redshift.

4.2 PDF of pseudo redshifts

4.2.1 Fitting with Gaussian-like distribution function

To apply pseudo redshifts in estimating H_0 , probability density distribution of pseudo redshift for each FRB is required. One simplest way to fit is to use a Gaussian distribution. However, an ordinary Gaussian distribution is symmetric while our samples are not necessarily symmetric. Also, Gaussian function extends to infinity in both directions, for example, we have $p(z \rightarrow \infty) > 0$ and $p(z < 0) > 0$, which obviously does not make sense in physical reality. To adapt Gaussian distribution to our usage, we must truncate Gaussian distribution.

There is an existing distribution called truncated normal distribution, which is a Gaussian-like function where variable is limited within a given region. It is implemented with such method: sample with an ordinary Gaussian distribution, and resample if the variable is out of boundary. It is easy to prove that this method does not change relative proportions of probability within allowed region, thus a truncated normal distribution is same as a cut-off Gaussian distribution which is "stretched" for normalization, and their PDF writes as:

$$f(x; \mu, \sigma, a, b) = \frac{1}{\sigma} \frac{\varphi\left(\frac{x-\mu}{\sigma}\right)}{\Phi\left(\frac{b-\mu}{\sigma}\right) - \Phi\left(\frac{a-\mu}{\sigma}\right)} \quad (a < x < b), \quad (14)$$

where $\phi(x)$ and $\Phi(x)$ are PDF and CDF of standard Gaussian distribution. With limitation parameters a and b , we can now introduce the asymmetry of original KDE into truncated normal distribution.

Taking FRB20180725A as an example, we plot Gaussian distribution and truncated normal distribution (limited within 1σ interval) in Fig. 3. Parameters for Gaussian distribution is $\mu = z_{50}, \sigma = (z_{84} - z_{16})/2$, and parameters for truncated normal distribution is $\mu = z_{50}, \sigma = (z_{84} - z_{16})/2, a = z_{16}, b = z_{84}$ where z_{16}, z_{50} and z_{84} are percentiles of pseudo redshifts. However, truncated normal distribution does not work well in MCMC simulation. The chain fails to converge after a long time of simulation. One possible reason is that the truncated function is too "flat" within 1σ region, and the difference is diluted. As shown in Fig. 3, the probability density around z_{84} is fairly high and its difference from peak probability is insignificant.

4.2.2 Sampling directly from MCMC results

In fact, the best way to describe pseudo redshift is using the KDE function, yet there is no analytic expression. Instead of looking for a probability function to fit the KDE as Section 4.2.1 does, sam-

pling directly from MCMC results is a more accurate yet more computational-costing way. For each FRB, the 57600 samples generated in Section 4.1 naturally follow the PDF of pseudo redshift, and randomly sampling from them will provide a statistical variable following the same PDF. Since such method requires much computation, we thin the samples with a ratio of 1:50 to greatly reduce the computation and also to avoid small-probability values. Our tests show that sampling among 1152 thinned samples gives results with little difference from original KDE function.

4.3 Simulation of unlocalized FRBs

With all data of pseudo redshifts for unlocalized FRBs prepared, difference still exists between simulation of localized and unlocalized FRBs. Generally there are two methods of simulating: integrating with entire probability density, and using randomly scattered pseudo redshifts, both of which are necessary to give a comprehensive understanding of constraint on Hubble constant.

4.3.1 Using integral of probability distribution

To get a more precise result on the estimated value of H_0 , the best way is to integrate pseudo redshifts within MCMC simulation. This will add another level of integral in Equation (9), which becomes:

$$\mathcal{L}_{\text{FRB}} = \int_0^\infty p(z) \int_0^{(1+z)DM_{\text{exc}}} p_{\text{host}}(DM_{\text{host}} | H_0) \times p_{\text{IGM}}(DM_{\text{exc}} - \frac{DM_{\text{host}}}{(1+z)} | H_0) d DM_{\text{host}} dz, \quad (15)$$

where $p(z)$ is normalized PDF of pseudo redshift. Obviously Equation (15) would significantly increase computation. An alternative method is to randomly pick one value for z following its PDF within each MCMC step. With $512 \times 2000 \sim 10^6$ steps for each FRB, it is reasonable to believe such sampling can well reflect probability distribution of pseudo redshifts. This greatly reduces computation compared with the former method, yet the values of redshift keep changing within a considerable range for each MCMC step, which makes the chain extremely hard to converge.

To avoid constant fluctuation of redshifts, we use median values of pseudo redshifts (blue dots in Fig. 2) in simulation. Median values indicate the expectation of probability distribution, and do not cause unacceptable computation or divergence of the chain.

4.3.2 Using randomly scattered pseudo redshifts

Despite the expectation of the probability distribution providing the most possible median value of H_0 that we would find if all FRBs were localized, it does not tell us about the uncertainty of the constraint. Assume that all FRBs have been localized and we try to constrain H_0 with their redshifts under these given circumstances:

- (a) the redshifts are found to be exactly the median values of our simulation (blue dots in Fig. 2);
- (b) the redshifts are found to randomly scatter around the median values following the probability distribution (red dots in Fig. 2).

The uncertainty of H_0 given by our hypothetical constraint under both conditions could be different. To be precise, (b) is most likely to give a constraint less tight than (a), thus results from Section 4.3.1 is not enough to predict the comprehensive result of constraint with unlocalized FRBs.

To simulate a condition described in (b), which is also more likely to actually happen than in (a), we assign a fixed value of redshift

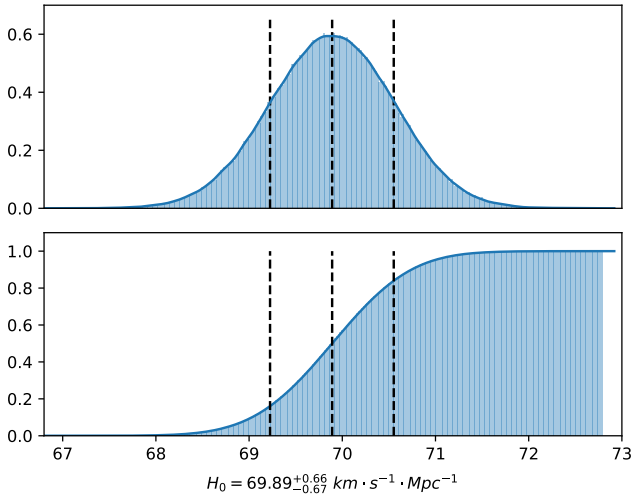


Figure 4. PDF and CDF of Hubble constant given by unlocalized FRBs. Median value of all samples generated by MCMC simulation is used as its redshift for each FRB. Vertical line shows the result $H_0 = 69.89^{+0.66}_{-0.67} \text{ km s}^{-1} \text{ Mpc}^{-1}$ with 1σ uncertainty.

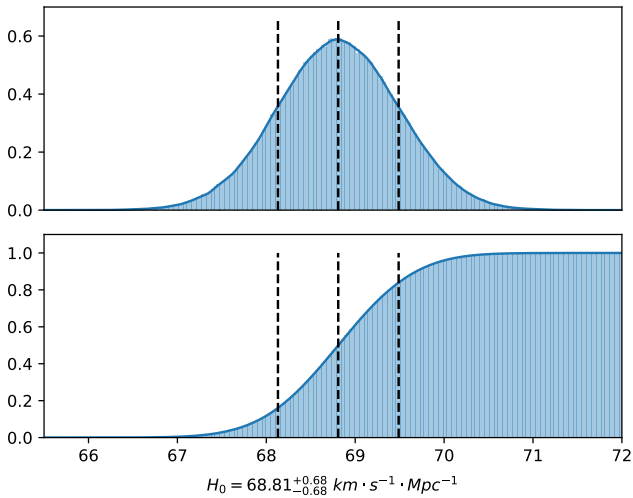


Figure 5. PDF and CDF of Hubble constant given by estimated pseudo redshift of unlocalized FRBs as shown in Fig 1 (red dots). Vertical line shows the result $H_0 = 68.81^{+0.68}_{-0.68} \text{ km s}^{-1} \text{ Mpc}^{-1}$ with 1σ uncertainty.

for each FRB by randomly scattering values following the PDF of pseudo redshifts around the median value. After discussions in Section 4.2, we directly sample from MCMC simulation samples to get a value which follows the PDF instead of fitting the KDE function. By sampling "around the median value", we mean that extreme samples (below 3% or above 97%) from MCMC simulation are discarded, and we only sample from the rest 94% interval. The scattered values are shown as red dots in Fig. 2.

4.3.3 Results of unlocalized FRBs

We run MCMC simulation in a way most similar to Section 3 with different pseudo redshift values as described in Sections 4.3.1 and 4.3.2. Simulation with median redshifts gives a 68% confidence interval of $H_0 = 69.89^{+0.66}_{-0.67} \text{ km s}^{-1} \text{ Mpc}^{-1}$ as shown in Fig. 4. Simulation with

scattered redshifts gives $H_0 = 68.81^{+0.68}_{-0.68} \text{ km s}^{-1} \text{ Mpc}^{-1}$ as shown in Fig. 5. The results differ slightly in expectation of H_0 , yet show little difference in uncertainty.

The median value seems to deviate from the median value constrained with localized FRBs, yet still lies in the 1σ confidence interval in Fig. 1. In comparison, since the redshifts are "pseudo", the uncertainty of result from unlocalized FRBs is much more inspiring than the median value. It provides a convincing prediction that if all 527 FRBs are localized, the uncertainty will drop to $\sim 1\%$ at 1σ confidence. Compared with result of localized FRBs, we have $e_1/e_2 = 3.38$ and $\sqrt{N_2}/\sqrt{N_1} = 2.76$. The ratios slightly deviate from the relation $e \sim 1/\sqrt{N}$. A possible explanation is that the number of localized FRBs is still limited, and the real redshift distribution does not exactly follow the relation we simulated.

5 DISCUSSION

By introducing 527 unlocalized CHIME FRBs and using scattered pseudo redshifts, the uncertainty of constraint is significantly reduced. However, some bias and error must be included for a full discussion. We generally divide them into statistical error and systematic error.

5.1 Statistical error

Statistical error mainly refers to the error of cosmological parameters $\Omega_b h^2$ and Ω_m appeared in Equation (5). The error of f_{IGM} will be discussed in Section 5.2, and other constant in Equation (5) such as G and m_p are already measured with extremely high precision. Planck Collaboration et al. (2020) gave $\Omega_b h^2 = 0.02242 \pm 0.00014$ and $\Omega_m = 0.3111 \pm 0.0056$.

For $\Omega_b h^2$, it appears in Equation (5) as a linear term. Assuming a Gaussian distribution $p(x)$ around $\mu = 0.02242$, we can do a rough estimation:

$$H_0 \sim \frac{\Omega_b h^2}{\langle \text{DM}_{\text{IGM}} \rangle} \sim \int_{-\infty}^{\infty} \frac{x}{\langle \text{DM}_{\text{IGM}} \rangle} p(x) dx \sim \frac{\mu}{\langle \text{DM}_{\text{IGM}} \rangle}, \quad (16)$$

which shows a symmetric distribution of $\Omega_b h^2$ has little influence on H_0 . Furthermore, the precision of $\Omega_b h^2$ ($\sim 0.6\%$) is slightly smaller than that of H_0 of our constraint ($\sim 0.94\%$).

For Ω_m , which appears inside the integral in Equation (5), it has an uncertainty of $\sim 1.8\%$ and could not be ignored. To marginalize Ω_m , the best way is to add another level of integral, which would significantly increase computation. Alternatively, we consider replacing integral with expansion. Assume a Gaussian distribution $p(x)$ with $\mu = 0.3111$, $\sigma = 0.0056$, the integral can be wrote as:

$$\begin{aligned} I &= \int_{-\infty}^{\infty} p(x) \int_0^Z \frac{(1+z)}{[x(1+z)^3 + 1-x]^{1/2}} dz dx \\ &\approx \int_0^Z \frac{(1+z)}{I_0} \int_{\mu-\sigma}^{\mu+\sigma} \frac{p(x)}{[x(1+z)^3 + 1-x]^{1/2}} dx dz \\ &\equiv \int_0^Z \frac{(1+z)}{I_0} \int_{\mu-\sigma}^{\mu+\sigma} f(x, z) dx dz, \end{aligned} \quad (17)$$

where $I_0 = \int_{\mu-\sigma}^{\mu+\sigma} p(x) dx = 0.683$ is the normalization factor and $f(x, z) = p(x)/[x(1+z)^3 + 1-x]^{1/2}$ is our target function. Note that Z is redshift of FRB, and z is our integration variable. Since both $\int f(x, z) dx$ and $\int f(x, z) dz$ could not be expressed by elementary functions, we perform a series expansion on $f(x, z) dz$ around $x = \mu$

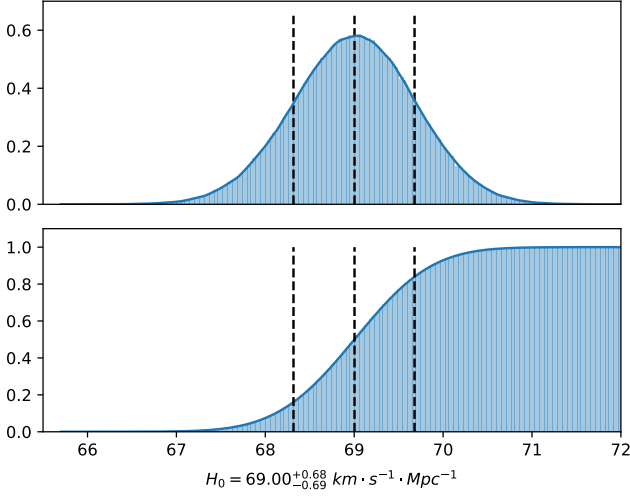


Figure 6. PDF and CDF of Hubble constant considering statistical error of Ω_m using estimated pseudo redshift of unlocalized FRBs. Vertical line shows the result $H_0 = 69.00^{+0.68}_{-0.69} \text{ km s}^{-1} \text{ Mpc}^{-1}$ with 1σ uncertainty.

and get $g(x, z) = \sum_{i=0}^5 a_i(z)(x - \mu)^i$. We plot the figure of $g(x, z)$ at different z and compare it with original function to ensure the expansion is acceptable. Now the inner integral in Equation (17) can be wrote as an explicit function of z , i.e. $h(z) = \int_{\mu-\sigma}^{\mu+\sigma} g(x, z) dx$. However, the form of $h(z)$ is still too complicated to integrate, thus we need to do another series expansion around $z = z_0$. To determine the best value for z_0 , we plot the expanded function at different z_0 and degrees. It is found that expanding $h(z)$ to the term of $(z - z_0)^4$ around $z_0 = 2.5$ provides best fit for both $z \rightarrow 0$ and $z \rightarrow 4$. Denote it as $j(z) = \sum_{i=0}^4 b_i(z)(z - z_0)^i$, and we can complete the whole integral: $I \approx 1.02 Z + 0.19 Z^2 - 0.14 Z^3 + 0.043 Z^4 - 0.0066 Z^5 + 0.00042 Z^6$.

Taking the new expression into Equation (5), we could run MCMC simulation with Ω_m marginalized. The result is shown in Fig. 6 (we use the method in Section 4.3.2). The 1σ confidence interval of H_0 is $69.00^{+0.68}_{-0.69} \text{ km s}^{-1} \text{ Mpc}^{-1}$ and has little difference with previous result in Fig. 5, which indicates that the statistical error of Ω_m does not influence constraint on H_0 significantly.

5.2 Systematic errors

There are several systematic errors that need to be discussed. In Equation (5), compared with $\Omega_b h^2$ and Ω_m , the fraction of baryon in IGM f_{IGM} may introduce more uncertainty. However, we still know little about f_{IGM} . Shull et al. (2012) gave the value of ~ 0.84 yet does not propose the errorbar. Connor et al. (2024) provided a more accurate constraint, yet it depends on several other models and theories. Furthermore, it is difficult for any constraint using Equation (5) to separate the error of f_{IGM} from H_0 as they appear in a coupling term f_{IGM}/H_0 in Equation (5). To be precise, only constraint on f_{IGM}/H_0 can be made instead of constraint on H_0 . So, the value of H_0 must be determined by other approaches when constraining f_{IGM} from FRBs. By fixing H_0 , it has been found that the uncertainty of f_{IGM} is about 8% (Yang et al. 2022; Connor et al. 2024). Obviously, the systematic error from f_{IGM} dominates the error of measured H_0 at present. On the other hand, it may varies with redshift. Researches with other methods are needed to further investigate the error of f_{IGM} .

DM_{host} includes all contributions to DM that come from FRB host galaxy. Using IllustrisTNG simulations, the probability distribution

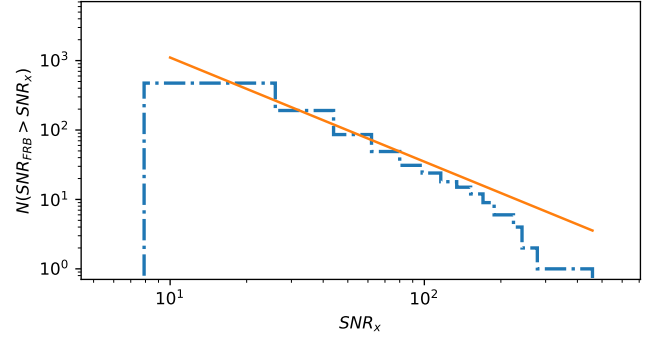


Figure 7. Log-log histogram of SNR for one-off FRBs in CHIME catalog where repeated FRBs are not counted. Yellow line with slope of -1.5 (in log-log scale) is not fitted by the data and just for comparison.

of DM_{host} including the local cosmic structure (e.g. filament) halo and interstellar medium of the host have been derived (Zhang et al. 2020). However, the vicinity environment of FRB progenitors have not been considered. The most promising progenitors of FRBs are young magnetars, which can be formed by core-collapse of massive stars or mergers of two compact objects (Wang et al. 2020). So they may be embedded in a magnetar wind nebula and supernova remnant (Yang & Zhang 2017; Piro & Gaensler 2018; Zhao & Wang 2021). Meanwhile, the largest DM_{host} with rotation measure reversal for FRB 20190520B indicates it may reside in a binary system (Wang et al. 2022; Anna-Thomas et al. 2023). So similar FRBs should be removed when measuring H_0 . For FRBs with little DM contribution from vicinity environment, precise modelling should be performed. It is important to use optical observations of the FRB host galaxy environment, combined with the rotation measure and scattering times of FRBs to constrain DM_{host} (Cordes et al. 2022).

Several selection biases should be discussed, such as SNR effect, ISM effect, selection effect of unlocalized FRBs and gridding effect (James et al. 2022). For the latter two effects, our constraint has no such error since we make use of most unlocalized FRBs in CHIME database and use continuous value for redshift and dispersion measures instead of discrete variables. For SNR effect, the log-log figure of number of events observed above SNR threshold should follow power law of -1.5 (in log-log plot, i.e. $N \propto \text{SNR}^{-1.5}$), and James et al. (2022) found that events from CRAFT/ICS deviates from the -1.5 power law. We plot the same figure with unlocalized FRBs from CHIME database in Fig. 7, and the histogram followed the power law well, thus our constraint is not much influenced by SNR effect. Finally, for the ISM effect, James et al. (2022) claimed that DM_{ISM} would increase at low galactic latitude, which may prevent telescopes from observing such events. We plot Hammer projection of FRBs in galactic coordinate system in Fig. 8. Hammer projection is an equal-area projection and there are a considerable amount of FRBs located in low galactic latitude area. Furthermore, few of these low-galactic-latitude FRBs have shown extreme values of DM_{ISM} even above 200 pc cm^{-3} . Thus ISM effect could be ignored during our constraint using unlocalized FRBs.

6 CONCLUSIONS

We run MCMC simulations to constrain Hubble constant using 69 localized FRBs and 527 unlocalized FRBs from CHIME catalog respectively. We apply redshift-dispersion measure relation and Bayesian estimation to build MCMC model. We use normalization

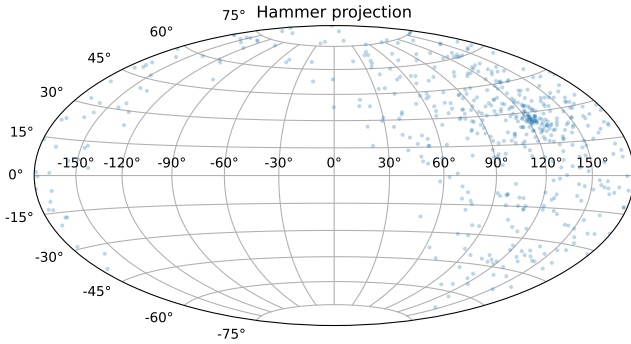


Figure 8. Hammer projection of distribution of FRBs in CHIME catalog on the celestial sphere in galactic coordinate system. Repeating FRBs are only counted once.

factors obtained from IllustrisTNG simulation to model DM distribution. For localized FRBs, we get the result of $H_0 = 70.41^{+2.28}_{-2.34}$ $\text{km s}^{-1}\text{Mpc}^{-1}$ with 69 FRBs, which lies between constraints from late-time and early-time research, further proving FRB to be an individual cosmological probe. For unlocalized FRBs, we run individual MCMC simulation instead of maximum likelihood estimation to get probability density distribution of pseudo redshift for each FRB. We use direct sampling instead of fitting kernel density estimation function to draw samples of pseudo redshifts. We combine two different methods of using pseudo redshifts to get a comprehensive constraint on Hubble constant, i.e. to use median value of redshifts and to use fixed scattered redshifts, which gives the result of $H_0 = 69.89^{+0.66}_{-0.67}$ $\text{km s}^{-1}\text{Mpc}^{-1}$ and $H_0 = 68.81^{+0.68}_{-0.68}$ $\text{km s}^{-1}\text{Mpc}^{-1}$ respectively.

We discuss statistical errors of cosmological parameters and systematic errors of f_{IGM} and selection biases. We show that the statistical error of Ω_b has a minor influence on our constraint compared to Ω_m , and we perform a series expansion to marginalize Ω_m and obtain the result of $H_0 = 69.00^{+0.68}_{-0.69}$ $\text{km s}^{-1}\text{Mpc}^{-1}$. We find that the coupling effect prevents us from separate the error of f_{IGM} from H_0 . The uncertainty of H_0 is dominated by the error of the fraction of cosmic baryons in diffuse ionized gas f_{IGM} . Other systematic errors could be neglected.

Our study gives a prediction of future constraint on Hubble constant with more localized FRBs. Our result shows that the uncertainty of Hubble constant is likely to drop to $\sim 1\%$ if the number of localized FRBs is raised to ~ 500 . We believe that with more samples localized, FRBs will become a powerful individual tool to solve Hubble Tension.

ACKNOWLEDGEMENTS

This work was supported by the National Natural Science Foundation of China (grant No. 12273009), the National SKA Program of China (grant No. 2022SKA0130100), the China Manned Space Project (CMS-CSST-2021-A12) and the Natural Science Foundation of Xinjiang Uygur Autonomous Region (grant No. 2023D01E20).

DATA AVAILABILITY

The data used is shown in Table 1 and relevant references.

REFERENCES

- Anna-Thomas R., et al., 2023, *Science*, **380**, 599
 Bannister K. W., et al., 2019, *Science*, **365**, 565
 Bhandari S., Flynn C., 2021, *Universe*, **7**
 Bhandari S., et al., 2020, *ApJ*, **895**, L37
 Bhandari S., et al., 2022, *AJ*, **163**, 69
 Bhandari S., et al., 2023, *ApJ*, **948**, 67
 Bhardwaj M., et al., 2021, *ApJ*, **919**, L24
 Bhattacharya M., Kumar P., Linder E. V., 2021, *Physical Review D*, **103**, 103526
 CHIME/FRB Collaboration et al., 2021, *ApJS*, **257**, 59
 Caleb M., et al., 2023, *MNRAS*, **524**, 2064
 Cassanelli T., et al., 2023, A fast radio burst localized at detection to a galactic disk using very long baseline interferometry ([arXiv:2307.09502](https://arxiv.org/abs/2307.09502))
 Chatterjee S., et al., 2017, *Nature*, **541**, 58
 Chime/Frb Collaboration et al., 2023, *ApJ*, **947**, 83
 Chittidi J. S., et al., 2021, *ApJ*, **922**, 173
 Connor L., et al., 2024, A gas rich cosmic web revealed by partitioning the missing baryons ([arXiv:2409.16952](https://arxiv.org/abs/2409.16952)), <https://arxiv.org/abs/2409.16952>
 Cooke R. J., Pettini M., Steidel C. C., 2018, *ApJ*, **855**, 102
 Cordes J. M., Chatterjee S., 2019, *Annual Review of Astronomy and Astrophysics*, **57**, 417
 Cordes J. M., Lazio T. J. W., 2002, [arXiv e-prints, pp astro-ph/0207156](https://arxiv.org/abs/astro-ph/0207156)
 Cordes J. M., Ocker S. K., Chatterjee S., 2022, *ApJ*, **931**, 88
 Deng W., Zhang B., 2014, *ApJ*, **783**, L35
 Driessen L. N., et al., 2023, *MNRAS*, **527**, 3659
 Freedman W. L., 2021, *ApJ*, **919**, 16
 Gao J., Zhou Z., Du M., Zou R., Hu J., Xu L., 2024, *MNRAS*, **527**, 7861
 Goodman J., Weare J., 2010, *Communications in Applied Mathematics and Computational Science*, **5**, 65
 Gordon A. C., et al., 2023, The Demographics, Stellar Populations, and Star Formation Histories of Fast Radio Burst Host Galaxies: Implications for the Progenitors ([arXiv:2302.05465](https://arxiv.org/abs/2302.05465)), <https://arxiv.org/abs/2302.05465>
 Hagstotz S., Reischke R., Lilow R., 2022, *MNRAS*, **511**, 662
 Heintz K. E., et al., 2020, *ApJ*, **903**, 152
 Hu J.-P., Wang F.-Y., 2023, *Universe*, **9**, 94
 Hubble E., 1929, *Proceedings of the National Academy of Science*, **15**, 168
 James C. W., et al., 2022, *MNRAS*, **516**, 4862
 Kalita S., Bhatporia S., Weltman A., 2024, Fast Radio Bursts as probes of the late-time universe: a new insight on the Hubble tension ([arXiv:2410.01974](https://arxiv.org/abs/2410.01974)), <https://arxiv.org/abs/2410.01974>
 Keane E. F., Stappers B. W., Kramer M., Lyne A. G., 2012, *MNRAS*, **425**, L71
 Kirsten F., et al., 2022, *Nature*, **602**
 Kumar P., Linder E. V., 2019, *Physical Review D*, **100**, 083533
 Law C. J., et al., 2020, *ApJ*, **899**, 161
 Law C. J., et al., 2024, Deep Synoptic Array Science: First FRB and Host Galaxy Catalog ([arXiv:2307.03344](https://arxiv.org/abs/2307.03344))
 Li Z., Gao H., Wei J. J., Yang Y. P., Zhang B., Zhu Z. H., 2020, *MNRAS*, **496**, L28
 Lin H.-N., Zou R., 2023, *Monthly Notices of the Royal Astronomical Society*, **520**, 6237
 Lin H.-N., Tang L., Zou R., 2023, *Monthly Notices of the Royal Astronomical Society*, **520**, 1324
 Lorimer D. R., Bailes M., McLaughlin M. A., Narkevic D. J., Crawford F., 2007, *Science*, **318**, 777
 Macquart J. P., et al., 2020a, *Nature*, **581**, 391
 Macquart J. P., et al., 2020b, *Nature*, **581**, 391
 Mahony E. K., et al., 2018, *The Astrophysical Journal Letters*, **867**, L10
 Marcote B., et al., 2020, *Nature*, **577**, 190
 McQuinn M., 2013, *ApJ*, **780**, L33
 Michilli D., et al., 2023, *ApJ*, **950**, 134
 Muñoz J. B., Kovetz E. D., Dai L., Kamionkowski M., 2016, *Physical Review Letters*, **117**, 091301
 Niu C.-H., et al., 2022, *Nature*, **606**, 873

- Ocker S. K., Cordes J. M., Chatterjee S., 2021, *ApJ*, 911, 102
- Petroff E., Hessels J. W. T., Lorimer D. R., 2022, *A&ARv*, 30, 2
- Pillepich A., et al., 2017, *MNRAS*, 473, 4077
- Piro A. L., Gaensler B. M., 2018, *ApJ*, 861, 150
- Planck Collaboration et al., 2020, *A&A*, 641, A6
- Prochaska J. X., Zheng Y., 2019, *MNRAS*, 485, 648
- Prochaska J. X., et al., 2019, *Science*, 366, 231
- Qiu X.-W., Zhao Z.-W., Wang L.-F., Zhang J.-F., Zhang X., 2022, *Journal of Cosmology and Astroparticle Physics*, 2022, 006
- Rajwade K. M., et al., 2022, *Monthly Notices of the Royal Astronomical Society*, 514, 1961–1974
- Ravi V., et al., 2019, *Nature*, 572, 352
- Ravi V., et al., 2022, *MNRAS*, 513, 982
- Ravi V., et al., 2023a, Deep Synoptic Array science: a 50 Mpc fast radio burst constrains the mass of the Milky Way circumgalactic medium ([arXiv:2301.01000](https://arxiv.org/abs/2301.01000))
- Ravi V., et al., 2023b, *ApJ*, 949, L3
- Riess A. G., et al., 2022, *ApJ*, 934, L7
- Ryder S. D., et al., 2023, *Science*, 382, 294
- Sharma K., et al., 2024, Preferential Occurrence of Fast Radio Bursts in Massive Star-Forming Galaxies ([arXiv:2409.16964](https://arxiv.org/abs/2409.16964)), <https://arxiv.org/abs/2409.16964>
- Shull J. M., Smith B. D., Danforth C. W., 2012, *ApJ*, 759, 23
- Tang L., Lin H.-N., Li X., 2023, *Chinese Physics C*, 47, 085105
- Tendulkar S. P., et al., 2017, *ApJ*, 834, L7
- Thornton D., et al., 2013, *Science*, 341, 53
- Valentino E. D., et al., 2021, *Classical and Quantum Gravity*, 38, 153001
- Walters A., Weltman A., Gaensler B. M., Ma Y.-Z., Witzemann A., 2018, *ApJ*, 856, 65
- Wang Y. K., Wang F. Y., 2018, *Astronomy & Astrophysics*, 614, A50
- Wang B., Wei J.-J., 2023, *ApJ*, 944, 50
- Wang F. Y., Wang Y. Y., Yang Y.-P., Yu Y. W., Zuo Z. Y., Dai Z. G., 2020, *ApJ*, 891, 72
- Wang H., Miao X., Shao L., 2021, *Physics Letters B*, 820, 136596
- Wang F. Y., Zhang G. Q., Dai Z. G., Cheng K. S., 2022, *Nature Communications*, 13, 4382
- Wang Y.-B., Zhou X., Kurban A., Wang F.-Y., 2024, *ApJ*, 965, 38
- Wei J.-J., Melia F., 2023, *ApJ*, 955, 101
- Wu Q., Wang F.-Y., 2024, *arXiv e-prints*, p. [arXiv:2409.13247](https://arxiv.org/abs/2409.13247)
- Wu Q., Yu H., Wang F. Y., 2020, *ApJ*, 895, 33
- Wu Q., Zhang G.-Q., Wang F.-Y., 2022, *MNRAS*, 515, L1
- Xiao D., Wang F., Dai Z., 2021, *Science China Physics, Mechanics, and Astronomy*, 64, 249501
- Yang Y.-P., Zhang B., 2017, *ApJ*, 847, 22
- Yang K. B., Wu Q., Wang F. Y., 2022, *ApJ*, 940, L29
- Yao J. M., Manchester R. N., Wang N., 2017, *ApJ*, 835, 29
- Zhang B., 2023, *Reviews of Modern Physics*, 95, 035005
- Zhang G. Q., Yu H., He J. H., Wang F. Y., 2020, *ApJ*, 900, 170
- Zhang Z. J., Yan K., Li C. M., Zhang G. Q., Wang F. Y., 2021, *ApJ*, 906, 49
- Zhao Z. Y., Wang F. Y., 2021, *ApJ*, 923, L17
- Zhao Z.-W., Zhang J.-G., Li Y., Zhang J.-F., Zhang X., 2022, *arXiv e-prints*, p. [arXiv:2212.13433](https://arxiv.org/abs/2212.13433)
- Zhou B., Li X., Wang T., Fan Y.-Z., Wei D.-M., 2014, *Physical Review D*, 89, 107303

This paper has been typeset from a $\text{\TeX}/\text{\LaTeX}$ file prepared by the author.